RESEARCH ARTICLE

Comprehensive molecular dynamics study of the role of Gln239/Arg238 residues in inhibiting hypoxia-inducible factor enzymes

Zhifei Zhu[1, 2, 3, *], Huirong Huang[3], Binxin Liu[3], Jing Huang[1, 2]

[1]Fujian Provincial Key Laboratory of Ecological Impacts and Treatment Technologies for Emerging Contaminants, College of Environmental and Biological Engineering, Putian University, Putian, Fujian, China. [2]Key Laboratory of Ecological Environment and Information Atlas, Fujian Provincial University, Putian, Fujian, China. [3]Fujian Zhixin Environmental Technology Co Ltd, Putian, Fujian, China.

Received: May 8, 2025; **accepted:** August 6, 2025.

Nonheme α-ketoglutarate-dependent (αKG-dependent) enzymes play pivotal roles in a variety of biochemical processes with factor inhibiting hypoxia-inducible factor (FIH) enzyme playing a pivotal role in mammalian oxygen homeostasis by hydroxylating Asn803 in hypoxia-inducible factor (HIF). While the catalytic center of FIH, which is coordinated by Fe(II)-αKG through His279, His199, and Asp201, has been the subject of extensive research, the precise influence of its secondary coordination sphere on hydroxylation, particularly the roles of Gln239 and Arg238, remains a significant challenge. This study utilized comprehensive molecular dynamic simulations to elucidate the biochemical attributes and functional significance of these secondary coordination sphere residues. The positioning of Fe-oxygen during O_2 activation and the positioning of the substrate C-terminal transcription activation domain (CTAD) Asn803 during hydrogen-atom abstraction (HAA) reactions were investigated in both wild-type and various mutant FIH enzymes including Gln239Ala, Gln239Asn, Gln239Glu, Gln239His, Gln239Leu, and Arg238Met. The results demonstrated that Gln239 played a pivotal role in modulating O_2 activation through the stabilization of reactive O_2 positioning in proximity to the Fe(II)-αKG center. Notably, mutations such as Gln239Leu had been reported to exert substantial detrimental effects on O_2 coordination and catalytic efficiency. In contrast, Arg238 played a critical structural role in orienting the HIF-1α CTAD-Asn803 substrate for optimal HAA by anchoring it near the active site. The absence of coordinating water molecules in proximity to the metal center served to emphasize the reliance of FIH on these secondary-sphere residues for precise catalytic control. These findings underscored a dual regulatory strategy, whereby Gln239 ensured efficient O_2 utilization during activation, and Arg238 facilitated substrate preorganization for HAA. This mechanistic understanding not only advanced fundamental knowledge of αKG-dependent hydroxylases but also offered promising avenues for engineering enzymes for therapeutic interventions for hypoxia-related conditions such as cancer and for innovations in fields such as medical wastewater treatment.

Keywords: hydroxylase factor-inhibiting hypoxia-inducible factor; microsolavated surroundings; molecular dynamics; Gln239/Arg238 variant.

[*]**Corresponding author:** Zhifei Zhu, Fujian Provincial Key Laboratory of Ecological Impacts and Treatment Technologies for Emerging Contaminants, College of Environmental and Biological Engineering, Putian University, Putian, Fujian 351100, China. Email: zhouh1313@163.com.

Introduction

Nonheme enzymes have been identified as critical catalysts in many biochemical reactions including hydroxylation, DNA/RNA repair, demethylation, and the synthesis and metabolism of various substances [1-3]. Among these enzymes, α-ketoglutarate-dependent

(αKG-dependent) nonheme enzymes play vital roles in human metabolism, participating in the synthesis of endogenous substances, the metabolism of exogenous drugs, and the regulation of physiological functions [4-6]. A notable member of this class is the factor inhibiting hypoxia-inducible factor (FIH), which is an iron-dependent αKG-dependent hydroxylase. FIH has been identified as a critical factor in maintaining oxygen homeostasis in mammals by facilitating the hydroxylation of Asn803 in hypoxia-inducible factor (HIF) [9]. HIF as a core transcription regulator is indispensable for the body's ability to sense oxygen concentrations and mount adaptive responses [9]. This catalytic mechanism mirrors those observed in other αKG-dependent iron-containing hydroxylases including TauD, AlkB, and SyrB2 [10, 11]. The hydroxylation of Asn803 by the FIH enzyme is initiated by the binding of O_2 to the Fe(II)-αKG site followed by O_2 activation, hydrogen atom abstraction, and rebound hydroxylation.

Significant advancements have been made in understanding the physiological and biochemical aspects of the FIH enzyme [12-19]. From a physiological perspective, HIF, in conjunction with its hydroxylase enzyme FIH, has emerged as a pivotal target for cancer therapy, offering potential mitigation for conditions associated with hypoxia (0.1 - 1% O_2) such as heart diseases, cancers, and strokes [12, 13]. From a biochemical perspective, the hydroxylation activity of the FIH factor demonstrates a high degree of sensitivity to its secondary coordination sphere. Research has demonstrated that mutations in residues such as Arg238, Gln239, and Asp201 result in significant limitations in hydroxylation [14]. The catalytic center of FIH is notably coordinated by Fe(II)-αKG through interactions with His279, His199, and Asp201 residues, forming a coordination geometry similar to that observed in the TauD and AlkB enzymes [16, 17]. A distinguishing characteristic of this active site structure is the notable absence of coordinating water molecules in the vicinity of the metal center. Furthermore, structural analysis revealed that the native HIF-1α polypeptide chain integrates into the FIH hydroxylase domain, positioning the asparagine residue within the C-terminal transcription activation domain (CTAD) directly above the catalytic site in a hydroxylated, inactive state. Experimental research has further clarified the crucial role of the secondary coordination sphere in the FIH hydroxylation process [18, 19]. Saban *et al*. highlighted the pivotal function of secondary sphere hydrogen bonds in facilitating the hydroxylation of Asn803 *via* the FIH factor. Subsequent studies further elucidated the role of hydrogen bonds from the Asn205, Asn294, Arg238, and Gln239 residues in promoting O_2 activation and ensuring accurate substrate positioning for hydroxylation [18]. In contrast to other αKG-dependent nonheme enzymes, Hangasky *et al*. demonstrated that, through steady-state kinetics analysis, the O_2 activation step was rate limiting during substrate hydroxylation [15]. Furthermore, mutating Gln239 to Ala, Asn, Glu, His, or Leu results in a decrease in the rate of O_2 activation and subsequent hydroxylation by the FIH factor [14]. In accordance with the previously mentioned findings, Iyer *et al*. underscored the pivotal role of the facial triad carboxylate in FIH in preserving the requisite structure for O_2 binding and the optimal position for CTAD Asn803 during the hydrogen–atom abstraction (HAA) reaction.

Despite these advances, a comprehensive understanding of how the microsolvation system precisely dictates the function and subsequent therapeutic manipulation of the hydroxylase FIH factor remains an ongoing challenge. The influence of the microsolvation environment of the enzyme has been thoroughly investigated experimentally. However, ensuring that these effects such as substrate positioning are accurately reproduced and comprehended through theoretical molecular dynamic simulations is imperative. A significant gap in existing knowledge is the lack of a comprehensive characterization of the biochemical attributes and the elucidation of the functional significance of the secondary coordination sphere within hydroxylation reaction mechanisms. This is particularly salient

with respect to the precise roles of key residues such as Gln239 and Arg238. The primary objective of this research was to characterize the biochemical attributes and elucidate the functional significance of the secondary coordination sphere within hydroxylation reaction mechanisms. The present study specifically focused on the Fe-oxygen position in O_2 activation and the position of the substrate CTAD Asn803 during HAA reactions to explore the key issues of hydroxylation in the wild-type FIH enzyme. Moreover, comprehensive theoretical molecular dynamic simulations were employed to investigate the microsolvation environment of the enzyme. Furthermore, the impact of specific mutations in the secondary coordination sphere including Gln239Ala, Gln239Asn, Gln239Glu, Gln239His, Gln239Leu, and Arg238Met on the hydroxylation process was rigorously examined. A comprehensive understanding of the pivotal function of the secondary coordination sphere in the oxygen regulation of FIH was paramount to elucidate its molecular mechanism in depth. This profound insight offered a promising avenue for future cancer therapy and bioengineering research. This knowledge also had significant implications for diverse fields including medical wastewater treatment and the development of new therapeutic strategies for Alzheimer's disease and related neuropsychiatric disorders.

Materials and methods

Systems setting up

X-ray crystallography data from Protein Data Bank (PDB) (https://www2.rcsb.org/) for the atomic coordinates of the FIH hydroxylase-HIF-1α polypeptide complex (PDB Code: 1H2L) and the substrate-free FIH structure (PDB Code: 1H2N) were obtained (Figure 1) [15]. Residues absent from the FIH factor (Met1 - Ala2 - Ala3 - Thr4 - Ala5 - Ala6 - Glu7 - Ala8 - Val9 - Ala10 - Ser11 - Gly12 - Ser13 - Gly14, Lys304 - Arg305 - Ile306) and the HIF-1α polypeptide chain (Ser786 - Met787 - Asp788 - Glu789 - Ser790 - Gly791 - Leu792 - Pro793 - Gln794) were subsequently incorporated by means of Modeler 10 (https://salilab.org/modeler/) [20]. According to the classification of molecules as detergents, the SO_4^{2-} ligands were eliminated from the initial structures.

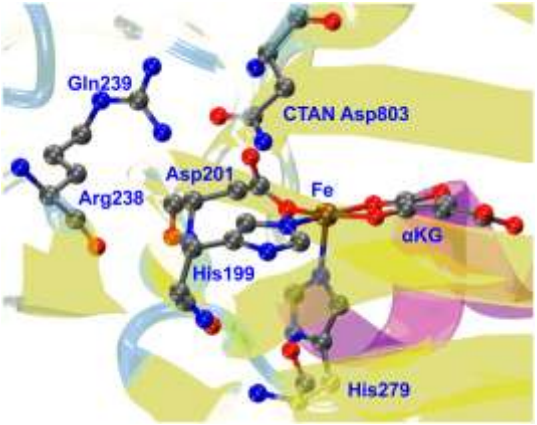

Figure 1. The active site of FIH factor with some essential groups highlighted.

The protonation states of acidic and basic residues were determined through visual inspection. Specifically, residues Glu54, Glu60, Glu130, Glu225, Glu307, Glu323, Asp28, Asp77, Asp89, Asp104, Asp134, and Asp248 were identified as protonated. The protonation states of the histidine residues were determined according to the following procedure that His98, His126, His199, His233, and His279 were assigned as the δ-N atom (HSD), while His234 and His280 were assigned as the ε-N atom (HSE) and His313 was assigned as the ε-δ-N atom (HSP).

Molecular simulation

After the docking procedure, missing hydrogen atoms were added to the system *via* the HBUILD module embedded in CHARMM (https://academiccharmm.org/) [21, 22]. The positions of these newly added hydrogen atoms were then subjected to 100 steps of adopted basis Newton-Raphson (ABNR) minimization to be optimized. To simulate the physiological environment, a water layer with a thickness of 18 Å was constructed around the enzyme *via* the VMD (https://www.ks.uiuc.edu/Research/vmd/)

Table 1. The statistics of snapshots with effective oxygen molecules in the substrate-containing and substrate-free FIH systems.

Systems	O_2 concentration	r ≤ 4.0 Å (%)	4.0 Å < r ≤ 4.4 Å (%)	r > 4.4 Å (%)	$\bar{r}$ (Å)
FIH (no sub.)	0.10%	8.0	12.2	79.8	5.29
	0.20%	24.1	16.0	59.9	4.83
	1.41%	49.1	31.2	19.7	4.09
FIH (with sub.)	0.10%	3.8	9.7	86.5	5.54
	0.20%	16.3	39.4	44.4	4.51
	1.12%	61.1	15.6	23.3	3.99

[23]. The innermost 8 Å of this solvent layer underwent minimization, first with 2,000 steps of ABNR followed by 500 steps of steepest descent (SD), and then equilibration by molecular dynamics (MD) for 50 ps at 300 K, while keeping the remainder of the system fixed. After the completion of the comprehensive solvation procedure, a productive molecular dynamics (MD) simulation of 50 ns was conducted for both the oxoferryl species and the ferric hydroxyl radical intermediate. The simulations employed the CHARMM36 force fields as implemented in the CHARMM program [22, 24]. During all MD simulations, the coordinates of the entire (αKGHis$_2$Asp)Fe...O_2 and (αKGHis$_2$Asp)Fe=O units, the metal-ligating residues, and the outer 8 Å of the solvent layer were maintained at a constant state to ensure the preservation of the catalytic site and its immediate environment.

The definition of reactive oxygen

To characterize the hydroxylation process with the requisite degree of accuracy, defining and identifying the reactive oxygen molecules within the FIH system are essential. In this work, "reactive oxygen molecules" were specifically defined as oxygen molecules situated at the catalytically active junction of the Fe site. The activation of these reactive oxygen molecules (O_2) by FIH functioned as a catalyst for the autohydroxylation process, which was subsequently triggered by these reactive O_2 molecules. To identify these reactive O_2 molecules throughout the MD trajectory, the shortest distances between the oxygen and iron (Fe) atoms of all relevant species were meticulously measured, which enabled the identification of a reactive region for oxygen and Fe binding, characterized by a distance of approximately 4.0 Å. Notably, this threshold was not intended to delineate the precise boundary of O_2 binding with Fe, rather, it was conceived as a practical means to differentiate between reactive and unreactive regions for the purpose of subsequent mechanistic investigations.

Results and discussion

O_2 activation

The probability of O_2 activation is directly proportional to the percentage of snapshots with reactive O_2 molecules appearing in the MD trajectory. According to the extant body of experimental evidence, O_2 activation has been demonstrated to occur in FIH in the absence of the substrate HIF-1α. In the present simulation, the role of the substrate HIF-1$alpha$ was the primary focus of this enzyme. O_2 activation did not occur in substrate-containing or substrate-free FIH enzymes under extremely low O_2 concentrations. This outcome was attributed to the fact that the majority of O_2 molecules were found to be more than 4.0 Å away from the active site at O_2 concentrations of 0.10% and 0.20% (Table 1). For the substrate-free FIH system at an O_2 concentration of 0.10%, a mere 8.0% of the snapshots exhibited reactive O_2 molecules (r < 4.0 Å) with an average Fe–O_2 distance of 5.29 Å. At an O_2 concentration of 0.20%, this figure increased to 24.1% with an average distance of 4.83 Å. Under hyperbaric conditions, for the substrate-free FIH enzyme, a 41% O_2 concentration was observed, and 49.1% of the snapshots presented reactive O_2 molecules with an average distance of 4.09 Å. In the substrate-containing FIH system, at 0.10% O_2, only 3.8% of

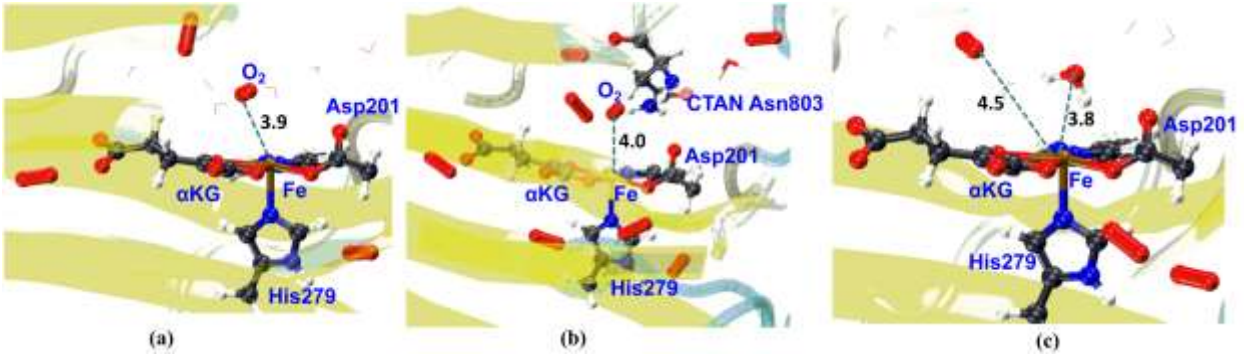

Figure 2. The representative snapshots in substrate-free FIH factor (**a**), substrate-containing FIH factor with reactive O_2 molecule (**b**), and the configuration of substrate-free FIH factor without reactive O_2 molecule (**c**). All distances shown were in Angstrom.

the snapshots presented reactive O_2 molecules with an average distance of 5 Å. An increase in the percentage of O_2 from 0.20% to 16.3% with an average distance of 4.51 Å was observed at 54 Å. O_2 molecules tended to remain within the substrate-containing FIH factor cavity as the O_2 concentration increased to 1.12%. The majority of the observed snapshots (61.1%) exhibited the configuration of reactive O_2 molecules, and an average Fe-O_2 distance of 3.99 Å was demonstrated. This finding was consistent with experimental observations, demonstrating that O_2 could be activated in both substrate-containing and substrate-free FIH. Furthermore, the microenvironment in proximity to the active site of enzymes was examined. The results showed that the configuration of reactive oxygen molecules in proximity to the active site of the substrate-containing and substrate-free FIH enzymes varied with distance. A representative snapshot of the substrate-free FIH factor with a reactive O_2 molecule was shown, where the distance between Fe and the reactive O_2 molecule was approximately 3.9 Å (Figure 2a). Likewise, a representative snapshot of the substrate-containing FIH factor with a reactive O_2 molecule was observed, where the Fe–O_2 distance was approximately 4.0 Å (Figure 2b). Conversely, when the Fe–O_2 distance increased to 4.5 Å, the O_2 molecule was maintained at a distance from the active site with a single water molecule positioned in the catalytically active junction of Fe (Figure 2c). This finding indicated that a distance of approximately 4.0 Å was optimal for the reactive O_2 molecules within the FIH enzyme system. To further investigate the roles of secondary sphere Gln239 and Arg238 residues in regulating O_2 reactivity during O_2 activation, the percentage of reactive O_2 molecules in the variant systems was examined. The statistical data concerning snapshots with effective oxygen molecules in the substrate-containing variant systems demonstrated that, in the variant systems, the majority of O_2 molecules were nonreactive, and the majority of snapshots did not exhibit reactive O_2 molecules. However, in the Gln239Ala variant, approximately 28.2% of the snapshots exhibited reactive O_2 molecules under hyperbaric conditions (1.12% O_2 concentration) with an average Fe–O_2 distance of 4.43 Å. Other variants presented a low probability of a reactive configuration (Table 2). The findings indicated that the Gln239Leu variant exhibited a marked reduction in O_2 activation with a mere 1.0% reactive configuration observed at a 1.12% O_2 concentration and an average Fe–O_2 distance of 6.23 Å, which suggested that the FIH systems underwent gradual activation by O_2 molecules in these variants. Furthermore, the secondary sphere Gln239/Arg238 residue was found to modulate the rate of O_2 activation. These results aligned with the experimental findings reported by Saban *et al*. Additionally, the percentage of snapshots containing reactive O_2 molecules reflected the rate of O_2 activation under hyperbaric conditions. It has been demonstrated that the greater the probability of a reactive configuration, the more

Table 2. The statistics of snapshots with effective oxygen molecules in the sub-containing variant systems.

FIH variants	O_2 concentration	r ≤ 4.0 Å (%)	4.0 Å < r ≤ 4.4 Å (%)	r > 4.4 Å (%)	$\bar{r}$ (Å)
Arg238Met	0.41%	2.2	6.8	91.0	6.81
	1.12%	5.6	15.9	78.5	5.14
Gln239Ala	0.41%	2.8	13.4	83.8	5.13
	1.12%	28.2	30.8	41	4.43
Gln239Asn	0.41%	5.0	20.6	74.4	5.03
	1.12%	8.6	33.0	58.4	4.71
Gln239His (δ-N protonated)	0.41%	1.4	9.0	89.6	5.37
	1.12%	6.6	28.7	64.7	4.75
Gln239Glu	0.41%	3.9	5.2	90.9	5.85
	1.12%	4.1	19.1	76.8	4.98
Gln239Leu	0.41%	0.1	0.0	99.9	6.88
	1.12%	1.0	2.9	96.1	6.23

rapid the O_2 activation. The percentage of reactive configurations and the experimentally measured O_2-activation rate exhibited a parallel sequence. The following amino acids were identified, which included Gln239Ala, Gln239Asn, Gln239His, Gln239Glu, and Gln239Leu. This finding suggested that Gln239 played a primary role in modulating O_2 activation through the stabilization of reactive O_2 positioning in proximity to the Fe(II)-αKG center. Mutations at this site such as Gln239Leu, disrupted O_2 coordination, resulting in a substantial impairment in catalytic efficiency.

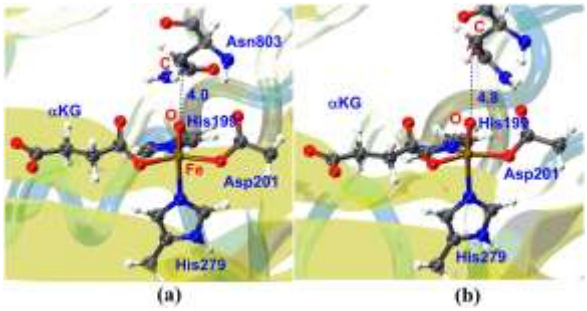

Figure 3. the representative snapshots with the Fe=O~C-Asn803 distance of 4.0 Angstrom (**a**) and larger than 4.0 Angstrom (**b**).

Hydrogen-atom abstraction

After O_2 activation, the substrate CTAD was situated in the appropriate location to enable Fe=O abstraction of a hydrogen atom from the methylene group at Asn803. A distance of 4.0 Å was determined to be optimal for the Fe=O~C-Asn803 interaction in the hydrogen-atom abstraction reaction (Figure 3). The term "reactive substrate positioning" was used to characterize the optimal position of the substrate and (αKGAspHis$_2$)Fe=O. In a manner analogous to the definition of a reactive O_2 molecule, a boundary of reactive substrate positioning and unreactive substrate positioning was determined, and the boundary of the Fe=O~C-Asn803 distance at 4.0 Å was selected. The statistics concerning reactive substrate positioning underscored the pivotal function of particular residues. In the wild-type FIH system, the CTAD Asn803 residue was found to be in the reactive position with an average distance of 3.31 Å, and the percentage of reactive substrate positioning was recorded as 100% when HIF-1α was present. In the absence of other substrate residues with only Asn, Asn803 was positioned at a distance of 6.23 Å from the active region, and only 2.5% of the snapshots exhibited reactive substrate positioning. Consequently, the side chain of the substrate HIF-1α polypeptide chain might play a pivotal role in maintaining the CTAD asparagine residue at an optimal position. Furthermore, the Arg238 residue was identified as a crucial element in maintaining the structural registry between the substrate and the active site. In the Arg238Met variant, Asn803 was positioned outside the reactive site. Only 4.1% of

Table 3. The statistics of snapshots with reactive substrate positioning in the wide-type and Arg238Met systems.

FIH systems	d ≤ 4.0 Å (%)	4.0 Å < d ≤ 4.4 Å (%)	d > 4.4 Å (%)	$\bar{d}$ (Å)
wt-FIH (with HIF-1α)	100	0.0	0.0	3.31
wt-FIH (with only Asn)	2.5	1.9	95.6	6.23
Arg238Met	4.1	50.4	45.5	4.37

Table 4. The statistics of snapshots with reactive substrate positioning in the Gln239 variants.

FIH systems	d ≤ 4.0 Å (%)	4.0 Å < d ≤ 4.4 Å (%)	d > 4.4 Å (%)	$\bar{d}$ (Å)
Gln239Ala	96.9	1.8	1.3	3.68
Gln239Asn	97.8	1.1	1.1	3.65
Gln239His (δ-N protonated)	98.2	0.8	1.0	3.65
Gln239Glu	91.0	7.3	1.7	3.75
Gln239Leu	65.4	32.4	2.2	4.00

the snapshots exhibited reactive substrate positioning with an average Fe=O~C-Asn803 distance of 4.37 Å (Table 3). This finding indicated a significant impairment in substrate orientation. In contrast, in all the Gln239 variants, the substrate was correctly positioned. The Fe=O ~ C-Asn803 distances varied from 3.65 Å (Gln239Asn and Gln239His) to 4.00 Å (Gln239Leu). The reactive substrate position accounted for 96.9% of the Gln239Ala variant and 97.8% of the Gln239Asn variant. Furthermore, a significant proportion of the snapshots, specifically more than 90%, were identified as reactive substrates positioned in the Gln239His (98.2%) and Gln239Glu (91.0%) variants. The reactive substrate position configuration was identified as the predominant substrate position in the Gln239Leu variant (65.4%) (Table 4). These findings were consistent with the experimental observations. Moreover, a comprehensive analysis of the reactive substrate positioning possibilities revealed that the Arg238 residue exerted a more significant influence on substrate positioning during hydrogen atom abstraction than did the Gln239 residue. This finding underscored the critical structural role of Arg238 in orienting the HIF-1α CTAD-Asn803 substrate for optimal HAA by anchoring the substrate in proximity to the active site. The absence of coordinated water molecules in proximity to the metal center further underscored the reliance of FIH on these second-sphere residues for precise catalytic control.

Mechanistic insights

This study elucidated the distinct functional roles of the Gln239 and Arg238 residues within the secondary coordination sphere of FIH hydroxylase through molecular dynamics simulations. The present findings demonstrated that Gln239 exerted its primary regulatory function by modulating O_2 activation, a process that involved the stabilization of reactive O_2 positioning in close proximity to the Fe(II)-αKG center. The presence of mutations at this particular site (e.g., Gln239Leu) had been observed to result in the disruption of O_2 coordination, thereby significantly impairing catalytic efficiency. In contrast, Arg238 played a critical structural role in orienting the HIF-1α CTAD-Asn803 substrate for optimal hydrogen-atom abstraction (HAA) by anchoring the substrate in proximity to the active site. The absence of coordinated water molecules near the metal center underscored the reliance of FIH on these secondary sphere residues for precise catalytic control. These mechanistic insights underscored the dual regulatory strategy of FIH, which was that Gln239 had been demonstrated to ensure efficient O_2 utilization during activation, whereas Arg238 facilitated substrate preorganization for HAA. The observed

sensitivity of FIH activity to mutations in these residues underscored its potential as a target for enzyme engineering to increase catalytic performance. From an applied perspective, the efficient O_2-utilization mechanisms of FIH could inspire innovations in medical wastewater treatment technologies, where optimizing oxygen dynamics was critical for degrading organic pollutants. Bioengineered FIH variants with enhanced O_2 affinity had the potential to improve the efficiency of aerobic treatment in hypoxic wastewater environments. Furthermore, this study emphasized the importance of molecular dynamics in elucidating the atomic-level mechanisms of enzyme catalysis, thereby establishing a framework for rational enzyme design in biotechnology and environmental remediation. The findings of this study contributed to the advancement of the fundamental understanding of αKG-dependent hydroxylases and facilitated the translation of enzymatic principles into sustainable engineering solutions.

Conclusion

These exhaustive molecular dynamics studies considerably enhanced the comprehension of the multifaceted functions of the secondary sphere Gln239 and Arg238 residues in modulating the catalytic activity of the hypoxia-inducible factor inhibitor (FIH) enzyme. The findings of this study elucidated a dual regulatory strategy that Gln239 had been found to primarily govern O_2 activation, whereas Arg238 had been identified as being crucial for optimal substrate positioning during hydrogen–atom abstraction (HAA). A comprehensive examination of the Fe–O_2 distances and reactive oxygen configurations was conducted to ascertain the role of Gln239 in regulating the efficiency of O_2 activation. The results demonstrated that Gln239 exerted a direct influence on the efficiency of O_2 activation by stabilizing the reactive O_2 molecule in proximity to the Fe(II)-αKG center. The present study corroborated experimental observations indicating that mutations at this site, particularly Gln239Leu, severely impaired O_2 coordination and catalytic efficiency, which underscored the critical function of Gln239 in the rate-limiting O_2 activation step. Conversely, the simulation results indicated that Arg238 played a pivotal structural role in anchoring the HIF-1α CTAD-Asn803 substrate in the precise orientation required for efficient HAA. The Arg238Met mutation significantly disrupted substrate positioning, thereby emphasizing its indispensable contribution to the formation of the catalytically competent enzyme–substrate complex. The notable absence of coordinating water molecules near the metal center further emphasized FIH's reliance on these secondary sphere residues for precise catalytic control. These mechanistic insights provided a foundation for rational enzyme design and engineering. By elucidating the mechanisms through which these specific residues modulated distinct steps in the hydroxylation pathway, targeted strategies might be developed to enhance or inhibit FIH activity, which had profound implications for various applications including the development of novel therapeutics for cancer and other hypoxia-related diseases, as well as inspiring innovative approaches in fields such as medical wastewater treatment through bioengineered enzymes with optimized oxygen utilization. The present study underscored the power of molecular dynamics simulations in unraveling atomic-level details of enzyme catalysis, paving the way for future advancements in both fundamental enzymology and applied biotechnology.

Acknowledgements

This research was supported by the Fujian Provincial Science and Technology Economic Integration Platform (Grant No. FJKX-2024XRH08), the Fujian Provincial Technological Innovation Key Research and Industrialization Projects (Grant No. 2023G019), the Science and Technology Plan Projects of Putian (Grant No. 2023GJGZ001, 2023GZ2001PTXY21), the National Innovation and Entrepreneurship

Training Program for College Students (Grant No. 202411498001X), and the Putian University Advanced Talents Startup Fund (Grant No. 2024042).

References

1. Wu C, Wang S, Sun D, Chen J, Ji W, Wang Y, *et al*. 2025. Nonheme manganese-catalyzed oxidative N-dealkylation of tertiary amides: Manganese (IV)-oxo aminopyridine cation radical species and hydride transfer mechanism. J Am Chem Soc. 147(13):11432-11445.
2. Yadav S, Lyons RS, Readi-Brown Z, Siegler MA, Goldberg DP. 2025. Influence of the second coordination sphere on O_2 activation by a nonheme iron (II) thiolate complex. J Inorg Biochem. 264:112776.
3. Yousefi MH, Masoudi A, Saberi Rounkian M, Mansouri M, Hojat B, Kaveh Samani M, *et al*. 2025. An overview of the current evidence on the role of iron in colorectal cancer: A review. Front Oncol. 15:1499094.
4. Hofmann A, Krajnc N, Dal-Bianco A, Riedl CJ, Zrzavy T, Lerma-Martin C, *et al*. 2023. Myeloid cell iron uptake pathways and paramagnetic rim formation in multiple sclerosis. Acta Neuropathol. 146(5):707-724.
5. Attri K, Chudasama B, Mahajan RL, Choudhury D. 2023. Therapeutic potential of lactoferrin-coated iron oxide nanospheres for targeted hyperthermia in gastric cancer. Sci Rep. 13(1):17875.
6. Bogoevska V, Wolters-Eisfeld G, Hofmann BT, El Gammal AT, Mercanoglu B, Gebauer F, *et al*. 2017. HRG/HER2/HER3 signaling promotes AhR-mediated Memo-1 expression and migration in colorectal cancer. Oncogene. 36(17):2394-2404.
7. Folgosa F, Tavares P, Pereira AS. 2015. Iron management and production of electricity by microorganisms. Appl Microbiol Biotechnol. 99(20):8329-8336.
8. Yin Y, Ren H, Wu H, Lu Z. 2024. Triclosan dioxygenase: A novel two-component rieske nonheme iron ring-hydroxylating dioxygenase initiates triclosan degradation. Environ Sci Technol. 58(31):13833-13844.
9. Pugh CW, Ratcliffe PJ. 2003. Regulation of angiogenesis by hypoxia: Role of the HIF system. Nat Med. 9(6):677-84.
10. Wang X, Tan X, Jian J, Zheng X, Zhao J, Huang J. 2024. O-B(F)←N functionalized copolymers with delayed fluorescence and P-type semiconducting characteristics. Macromol Rapid Commun. 45(16):e2400189.
11. Madayanad Suresh S, Zhang L, Hall D, Si C, Ricci G, Matulaitis T, *et al*. 2023. A deep-blue-emitting heteroatom-doped MR-TADF nonacene for high-performance organic light-emitting diodes. Angew Chem Int Ed Engl. 62(8):e202215522.
12. Semenza GL. 2009. Regulation of oxygen homeostasis by hypoxia-inducible factor 1. Physiology (Bethesda). 24:97-106.
13. Yabuki Y, Mitsuhashi A, Ogino H, Yoshida A, Nguyen NT, Yoneda H, *et al*. 2025. Hypoxia-inducible factor-targeting therapy augmented the sensitivity to programmed death ligand-1 blockade by enhancing interferon-γ-induced chemokines in tumor cells. Int J Cancer. 156(9):1814-1825.
14. Mingroni MA, Knapp MJ. 2021. Kinetic studies of the hydrogen atom transfer in a hypoxia-sensing enzyme, FIH-1: KIE and O_2 reactivity. Biochemistry. 60(44):3315-3322.
15. Elkins JM, Hewitson KS, McNeill LA, Seibel JF, Schlemminger I, Pugh CW, *et al*. 2003. Structure of factor-inhibiting hypoxia-inducible factor (HIF) reveals mechanism of oxidative modification of HIF-1 alpha. J Biol Chem. 278(3):1802-1806.
16. O'Brien JR, Schuller DJ, Yang VS, Dillard BD, Lanzilotta WN. 2003. Substrate-induced conformational changes in *Escherichia coli* taurine/alpha-ketoglutarate dioxygenase and insight into the oligomeric structure. Biochemistry. 42(19):5547-5554.
17. Li Q, Huang Y, Liu X, Gan J, Chen H, Yang CG. 2016. Rhein inhibits AlkB repair enzymes and sensitizes cells to methylated DNA damage. J Biol Chem. 291(21):11083-11093.
18. Saban E, Chen YH, Hangasky JA, Taabazuing CY, Holmes BE, Knapp MJ. 2011. The second coordination sphere of FIH controls hydroxylation. Biochemistry. 50(21):4733-4740.
19. Iyer SR, Chaplin VD, Knapp MJ, Solomon EI. 2018. O_2 activation by nonheme feII α-ketoglutarate-dependent enzyme variants: Elucidating the role of the facial triad carboxylate in FIH. J Am Chem Soc. 140(37):11777-11783.
20. Martí-Renom MA, Stuart AC, Fiser A, Sánchez R, Melo F, Sali A. 2000. Comparative protein structure modeling of genes and genomes. Annu Rev Biophys Biomol Struct. 29:291-325.
21. Brünger AT, Karplus M. 1988. Polar hydrogen positions in proteins: Empirical energy placement and neutron diffraction comparison. Proteins. 4(2):148-156.
22. Brooks BR, Brooks CL III, Mackerell AD, Nilsson L, Petrella RJ, Roux B, *et al*. 2009. CHARMM: The biomolecular simulation program. J Comp Chem. 30:1545-1615.
23. Humphrey W, Dalke A, Schulten K. 1996. VMD - visual molecular dynamics. J Molec Graphics. 14:33-38.
24. Huang J, Rauscher S, Nawrocki G, Ran T, Feig M, de Groot BL, *et al*. 2017. CHARMM36m: An improved force field for folded and intrinsically disordered proteins. Nat Methods. 14(1):71-73.